

**Strain-dependent insulating state and Kondo effect in epitaxial SrIrO<sub>3</sub> films**Gaurab Rimal <sup>1,2,\*</sup> Tanzila Tasnim <sup>1</sup> Gabriel Calderon Ortiz,<sup>3</sup>  
George E. Sterbinsky <sup>4</sup> Jinwoo Hwang <sup>3</sup> and Ryan B. Comes <sup>1,†</sup><sup>1</sup>*Department of Physics, Auburn University, Auburn, Alabama 36849, USA*<sup>2</sup>*Department of Physics, Western Michigan University, Kalamazoo, Michigan 49008, USA*<sup>3</sup>*Department of Materials Science and Engineering, Ohio State University, Columbus, Ohio 43210, USA*<sup>4</sup>*Advanced Photon Source, Argonne National Laboratory, Lemont, Illinois 60439, USA*

(Received 16 April 2024; accepted 13 June 2024; published 8 July 2024)

The large spin-orbit coupling in iridium oxides plays a significant role in driving novel physical behaviors, including emergent phenomena in the films and heterostructures of perovskite and Ruddlesden-Popper iridates. In this Letter, we study the role of epitaxial strain on the electronic behavior of thin SrIrO<sub>3</sub> films. We find that compressive epitaxial strain leads to metallic transport behavior, but a slight tensile strain shows gapped behavior. Temperature-dependent resistivity measurements are used to examine different behaviors in films as a function of strain. We find Kondo contributions to the resistivity, with stronger effects in films that are thinner and under less compressive epitaxial strain. These results show the potential to tune SrIrO<sub>3</sub> into Kondo insulating states and open possibilities for a quantum critical point that can be controlled with strain in epitaxial films.

DOI: [10.1103/PhysRevMaterials.8.L071201](https://doi.org/10.1103/PhysRevMaterials.8.L071201)

**Introduction.** The subtle role of quantum properties emerging from spin, charge, exchange, correlations, and topology brings about a plethora of unexpected emergent electronic behavior in quantum materials [1]. The large spin-orbit coupling (SOC) energy in 4*d* and 5*d* transition metal oxides (TMOs) compete with similar energy scales arising from other electronic degrees of freedom, including crystal-field splitting, magnetic coupling, and electronic correlations, which brings about a rich playground that helps realize new and unexpected electronic phases [2]. Furthermore, electron confinement and hybridization at the interface of heterostructures leads to emergent electronic states such as electron gases, superconductivity, magnetism, and quantum Hall states [3,4].

One interesting material system from the perspective of high spin-orbit coupling is the iridates [5,6]. These oxides, which have iridium as the main component, exhibit a subtle interplay between spin, orbit, charge, and crystallographic degrees of freedom, leading to competing electronic phases [7]. For example, the Ruddlesden-Popper (RP) series Sr<sub>*n*+1</sub>Ir<sub>*n*</sub>O<sub>3*n*+1</sub> comprises the insulating Sr<sub>2</sub>IrO<sub>4</sub> (*n* = 1), insulating Sr<sub>3</sub>Ir<sub>2</sub>O<sub>7</sub> (*n* = 2), and the semimetallic SrIrO<sub>3</sub> (*n* = ∞). The commonality of these systems is that they are correlated materials, and due to the large SOC imparted by Ir, are predicted or show phases such as superconductivity [8] and quantum paramagnetism [9]. Due to the large SOC from Ir, the *t*<sub>2*g*</sub> band effectively splits into *J*<sub>eff</sub> = 1/2 and *J*<sub>eff</sub> = 3/2 angular momentum states, and the Fermi level is positioned such that the ground state is a *J*<sub>eff</sub> = 1/2 paramagnetic semimetal [5]. Furthermore, Dirac nodes near the Fermi level provide

an avenue to tune electronic parameters which can result in metal-insulator transitions and novel magnetism [10].

The role of dimensionality in this RP series is also notable. As one goes from *n* = 1 (Sr<sub>2</sub>IrO<sub>4</sub>) to *n* = ∞ (SrIrO<sub>3</sub>), the magnetic property of the films changes, from an antiferromagnetic Mott insulator to a paramagnetic semimetal. However, BaIrO<sub>3</sub>, a hexagonal perovskite, is an insulator that shows ferromagnetism and charge density wave states [11]. The sensitivity to crystal symmetry thus drives the metallicity and magnetic behavior of these materials. Clearly, small changes imparted by thermodynamic or material parameters can dramatically change their properties.

A key challenge in studying novel phases is obtaining high-quality materials that are free from impurities and defects, such that disorder does not break symmetry and phase coherence. Improvements in material synthesis and characterization techniques have allowed the realization of many novel materials. Although bulk single crystals can be grown using traditional solid state synthesis techniques, thin films have the advantage of tuning the dimensionality, as well as the added benefits such as strain manipulation, delta and modulation doping, and Fermi level control via electrostatic gating. Molecular beam epitaxy (MBE) is a preferred method in thin-film growth and typically results in films with the best qualities [12]. The ability to control multiple degrees of freedom, combined with *in situ* characterization [13] and ultrahigh vacuum transfer to other probe stations, makes MBE the best technique to grow ultrahigh-quality materials. Although widely used in the semiconductor industry, it has now been well adapted for growth of oxides, and new improvements [14] have allowed the realization of materials in the 4*d* and 5*d* blocks of the periodic table that were previously quite difficult, if not impossible, to grow as thin films.

\*Contact author: gaurab.rimal@wmich.edu

†Contact author: ryan.comes@auburn.edu

The major difficulty in the MBE growth of iridates is the low vapor pressure of Ir, which can be circumvented by using a traditional electron-beam source [15] or a metal-organic source [16]. Here, we report the growth of SrIrO<sub>3</sub> using metal-organic MBE and show how epitaxial strain can be used to tune the electronic behavior of the material. Unlike previous reports, we show that a slight tensile strain leads to insulating behavior, whereas compressive strain leads to a metallic ground state. Furthermore, we observe a Kondo contribution to resistivity which scales with strain. We posit that strain in epitaxial SrIrO<sub>3</sub> films has a large role in the electronic behavior through tuning of oxygen vacancies. The observation of the Kondo effect that scales with strain hints at the proximity of the  $n = \infty$  phase to a magnetically ordered ground state.

**Experimental Methods.** We grew SrIrO<sub>3</sub> (SIO) films with varying thickness on LaAlO<sub>3</sub> (LAO), (La<sub>0.18</sub>Sr<sub>0.82</sub>)(Al<sub>0.59</sub>Ta<sub>0.41</sub>)O<sub>3</sub> (LSAT), SrTiO<sub>3</sub> (STO), and GdScO<sub>3</sub> (GSO) substrates using metal-organic MBE following a previously reported procedure [16]. The growth temperature was 650 °C, as monitored by a thermocouple placed behind the substrate. The oxygen plasma was kept at a pressure of  $6 \times 10^{-6}$  Torr and plasma was generated at a power of 300 W. The films were grown at a rate of approximately 1 Å/min, and were cooled under plasma at 10–20 °C/min.

Growth was monitored *in situ* using reflection high-energy electron diffraction (RHEED). Postgrowth, x-ray photoelectron spectroscopy (XPS) was done via UHV transfer to a PHI 5400 XPS system with a monochromatic Al  $K\alpha$  source using 17.9 eV pass energy and an electron flood gun neutralizing source. Binding energies were calibrated by aligning the primary O 1s peak to 530 eV [13]. *Ex situ* x-ray diffraction was done on the films using a Rigaku Smartlab with a Cu  $K\alpha$  anode, Ge(220) two-bounce monochromator, and two-dimensional (2D) detector. The film thickness was determined using x-ray reflectivity (XRR) and reciprocal space mapping (RSM) was used to determine in-plane epitaxial strain in relation to the substrate. Transport measurements were done using the dc van der Pauw method in a Quantum Design Dynacool system.

High angle annular dark-field (HAADF) images of a 10-nm-thick SIO sample grown on SrTiO<sub>3</sub> were acquired using a Thermo Fisher Themis Z scanning transmission electron microscopy (STEM) operated at 300 kV. Cross-sectional samples for STEM were prepared using a focused ion beam, with the initial milling at 20 keV and then subsequently at 5 keV. The samples were further cleaned using Fischione 1040 Nanomill with the ion beam energy of 500 eV before the STEM imaging. Ir  $L_3$  edge x-ray absorption spectra on a 14-nm-thick SIO/STO sample were collected at beamline 20-BM of the Advanced Photon Source at Argonne National Laboratory. The x-ray beam was focused by Pt/alumina bilayer coated toroidal mirror and monochromated by a pair of Si(111) crystals. The x-ray polarization was perpendicular to the film surface normal, and an angle of incidence of less than 10° was used. Spectra were collected while the sample was spun about the surface normal direction in order to mitigate Bragg scattering. A seven-element Ge solid state detector was used to collect the Ir  $L\alpha$  fluorescence emission as the incident energy was changed.

**Results and Discussion.** In Fig. 1, we show that high-quality epitaxial SIO films can be grown using metal-organic MBE. RHEED in Fig. 1(a) shows that the growth of SIO follows in layered fashion, with the film commensurate with the underlying substrate lattice. SIO has an orthorhombic phase in bulk with lattice constants  $a = 5.60$  Å,  $b = 5.58$  Å, and  $c = 7.89$  Å [17], and the pseudocubic lattice constant for the perovskite form is 3.953 Å. When grown on closely lattice-matched substrates, the film will be coherently strained, which is verified using RHEED and RSM as shown in Figs. 1(a) and 1(b). XRD in Fig. 1(c) shows that SIO grows as a single-phase film. STEM shows the good quality, sharp interface, and commensurate epitaxy of the SIO films in Fig. 1(d). The stoichiometry and proper layering is also confirmed by energy-dispersive x-ray spectroscopy as shown in Supplemental Figs. S1 and S2 [18]. XAS for Ir  $L_3$  edge is shown in Supplemental Fig. S3 [18] and confirms the Ir<sup>4+</sup> state [19,20].

Figure 2 shows the role of epitaxial strain on the SIO films. In Fig. 2(a), we compare XRD for the strained SIO films. GSO has a slight tensile strain (~0.2%) while STO, LSAT, and LAO result in compressive strains of 1.2%, 2.4%, and 4.3%, respectively. As the lattice constant of the substrates decrease from GSO to STO to LSAT to LAO, we observe an expansion in the  $c$ -axis lattice constant for films of the same thickness, as shown in Fig. 2(b). Since the lattice mismatch with LAO is large compared to LSAT, it is expected that strain relaxation will occur sooner for growth on LAO compared to better lattice-matched substrates, which is verified using RHEED and RSM as shown in Supplemental Fig. S4 [18]. As expected, we also observe that for the most highly strained films (on LAO), the relaxation occurs more quickly with thickness (between 3 and 5 nm) compared to films on the better-matched substrates. Strain will also lead to distortions and expansion in the  $c$ -axis lattice parameter which is exhibited in Fig. 2(a) where the film XRD peaks shift relative to the substrate peaks. Laue oscillations also confirm the excellent crystallinity and good layering in these films, and helps determine the film thickness. XPS measurements of the Ir  $4d$  core level show that the Ir electronic state do not change with strain, as shown in Fig. 2(c).

Figure 3 shows the electronic transport behavior of strained 5-nm-thick SIO films. In bulk SIO single crystals, the low-temperature resistivity is about 2.2  $\mu\Omega$  cm [21] and the resistivity of our films is comparable to previously reported values on films [15,16,22,23]. Both 300 and 5 K resistivities are comparable to the lowest on record for MBE-grown films using both metal-organic MBE [16] and electron-beam-assisted MBE [15], indicating the high crystalline quality and low extrinsic impurity concentrations of our films. It can be observed in Fig. 3(a) that the least strained film (on GSO) shows an insulating behavior whereas higher compressive strain leads to more metallic behavior. Higher compressive strain was also found to drive a more metallic behavior in SrIrO<sub>3</sub>/SrTiO<sub>3</sub> superlattices [24]. However, unlike previous cases of strained SrIrO<sub>3</sub> on GdScO<sub>3</sub> [22], all our films on GSO (up to 14 nm thick) show an insulating behavior but have lower resistivities at 300 K. First-principles calculations showed that tensile strain in SIO, which creates a longer bond distance, results in higher carrier hopping energies

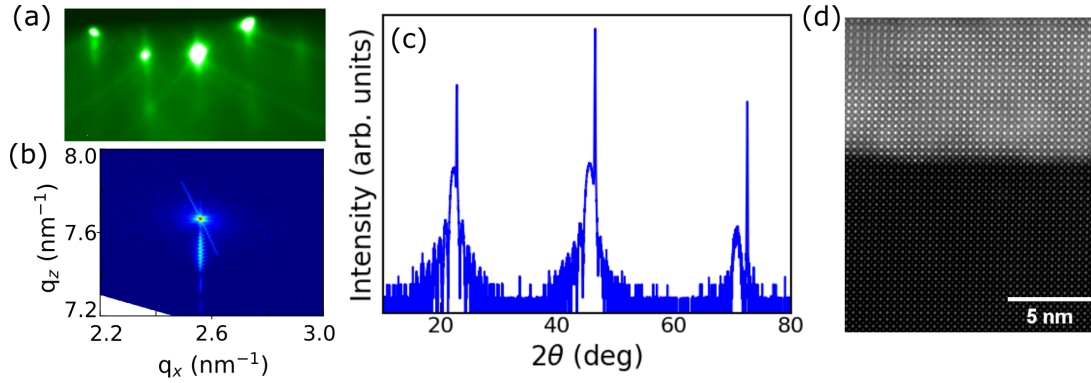


FIG. 1. Structural behavior of strained SrIrO<sub>3</sub> films grown on SrTiO<sub>3</sub>. (a) RHEED. (b) RSM for (103). (c) XRD. (d) Cross-sectional STEM.

[25], whereas the reverse can be expected in the case of compressive strain, which qualitatively explains the behavior. The metallic films show an upturn at lower temperatures (see Supplemental Fig. S5 [18]) which may be attributed to Kondo and weak antilocalization (WAL) (Supplemental Fig. S6 [18]) effects. A similar upturn in resistivity has been observed in other SIO films [16,23,26] but not much emphasis has been placed in understanding the origins or implications of this behavior. The general trend of  $\rho$  vs  $T$  shows a decreasing upturn temperature with increasing strain.

To understand the transport behavior, we modeled the resistivity with contributions from different scattering mechanisms. The temperature dependence of resistivity,  $\rho(T)$ , can be modeled using contributions [16,27,28] from impurity  $\rho_0$ , quasiparticle  $\rho_1$ , and Kondo scattering  $\rho_K$ , with an added contribution from WAL  $\rho_3$ , and given as

$$\rho(T) = \rho_0 + \rho_1 T^{1.4} + \rho_K \left( \frac{T_K'^2}{T^2 + T_K'^2} \right)^s - \rho_3 \log(T), \quad (1)$$

where  $T_K' = \sqrt{T_K/(2^{1/s} - 1)}$ ,  $s = 0.225$ , and  $T_K$  is the Kondo temperature [29]. This model fits our data well, as shown in Fig. 3(b). The strain dependence of the Kondo contribution to resistivity, as shown in Fig. 3(c) and Supplemental Fig. S7 [18], suggests the intricate role of strain in the Kondo scattering of charge carriers. The Kondo resistivity, which scales with the concentration of localized magnetic states [30], shows that the strain is responsible for the localized magnetic states that form in the system. Furthermore, as shown in Fig. 3(d), the Hall coefficient decreases with increasing

compressive strain, which suggests that the net carrier density increases at higher compressive strain.

We now discuss the nature of the local magnetic states in these films. Unlike in the case of CaCu<sub>3</sub>Ir<sub>4</sub>O<sub>12</sub>, wherein incipient Kondo behavior is present due to hybridization between localized Cu and itinerant Ir states [31], there are no clear localized magnetic states available in SIO. Extrinsic impurities are minimal in these films, as determined by XPS and Rutherford backscattering spectrometry (see Supplemental Figs. S8–S10 [18]) and comparisons to past MBE-grown films [15,16]. Oxygen vacancies have been predicted to drive ferromagnetism and Kondo behavior in SrTiO<sub>3</sub> [28,32] and have also been proposed as the cause of Kondo behavior of SrIrO<sub>3</sub> films grown using metal-organic MBE [16]. Thus, we propose that oxygen vacancies are the source of the local magnetic states and are largely responsible for the Kondo behavior. This prompts a question regarding the role of these localized states in the competition between different energy scales.

An insulating antiferromagnetic ground state was observed in nonstoichiometric SIO single crystals [33] and Sn-substituted SIO [34] and mechanisms such as carrier doping and chemical pressures were proposed to drive this transition. Density functional theory (DFT) calculations have shown that strain has a large role on the oxygen vacancy formation energy [35], with tensile strain leading to higher vacancy formation. Similarly, DFT showed the role of epitaxial strain and oxygen vacancies in Sr<sub>3</sub>Ir<sub>2</sub>O<sub>7</sub> [36], in which tensile and compressive strain favored antiferromagnetic couplings in both in-plane and out-of-plane directions, and also found

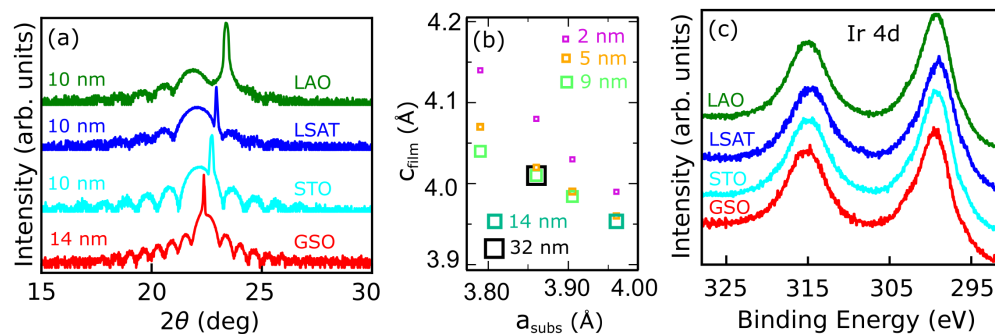


FIG. 2. Comparison of SIO films on different substrates. (a) XRD for (001) peaks. (b) The variation of  $c$ -axis lattice constant with the substrate and the thickness. (c) Ir 4d XPS spectra for 2-nm-thick films.

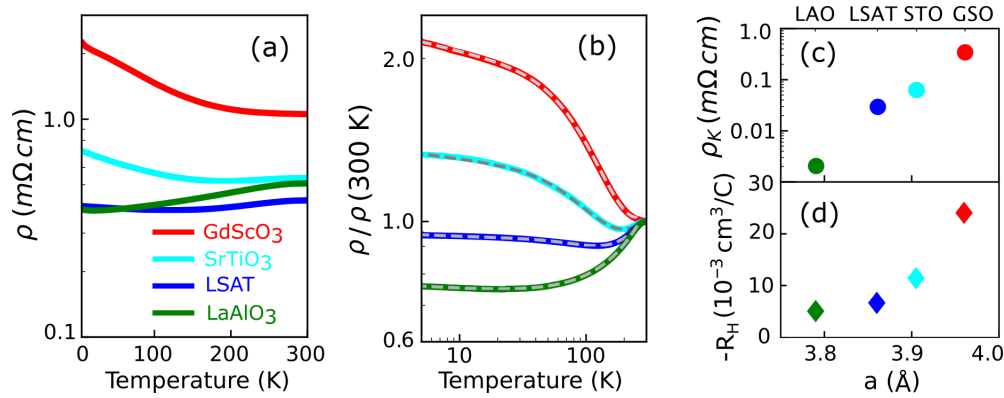


FIG. 3. Transport behavior of 5-nm-thick SrIrO<sub>3</sub> films. Temperature dependence of (a) resistivity, and (b) resistivity normalized to the room-temperature value. The dashed lines in (b) show fits to the transport model defined in Eq. (1). (c) Kondo scattering term extracted from fits in (b). (d) Hall coefficient at 5 K.

that compressive strain favored higher oxygen vacancies. Very recently, the same conclusion was found in SrIrO<sub>3</sub> films [37]. The observation of an antiferromagnetic ground state in compressively strained SrIrO<sub>3</sub>/SrTiO<sub>3</sub> superlattices [24,38] may also be intimately related to the effect of vacancies. It should also be pointed out that due to the similar energy scales there may be large changes in the electronic and magnetic behavior, which is why different reports or preparation methods lead to different film behaviors.

Another comment on the transport behavior is on the non-Fermi-liquid (NFL) contribution to the resistivity. Ferromagnetic instability close to the NFL state was found in bulk single crystals of SIO, which lies close to a quantum critical point [21]. Cui *et al.* [34] found that Sn-substituted SrIrO<sub>3</sub> shows antiferromagnetic order and a gap opening below the transition temperature, and antiferromagnetic order was also found for nonstoichiometric SIO [33]. Transport and STM studies also revealed a small gap around 60 meV in SIO confined between SrTiO<sub>3</sub> [26], which was attributed to antiferromagnetic order through DFT calculations. Antiferromagnetic order has also been demonstrated using x-ray magnetic scattering in SIO/SrTiO<sub>3</sub> superlattices [24,39]. The observation of Kondo behavior in our films may thus be a precursor to a magnetic state in strained SIO films.

We also investigate the role of thickness and strain relaxation in a series of films grown on LSAT substrates, as shown

in Fig. 4. The 32-nm film is partially relaxed, while the others are coherently strained. The film with the lowest thickness shows a fully insulating behavior whereas other films exhibit metallic behavior. Except for the 9-nm-thick film the other films show an upturn when cooled and the thickest film has a higher resistivity compared to the next thickest film. Among the thinner films, surface scatterings or increased oxygen vacancy concentrations near the film surface are also likely to result in higher resistivity and Kondo effects, thereby leading to the lowest resistivity in the 9-nm-thick film. The presence of misfit dislocations in the thicker film may help to explain the low-temperature upturn, given that oxygen vacancies are known to accumulate at dislocations in complex oxide films [40].

Magnetoconductance, shown in Fig. 4(c) and Supplemental Fig. S6 [18], also verifies the WAL nature in the films, which fits well with the Hikami-Larkin-Nagaoka (HLN) model [41], showing the large role of spin-orbit coupling in SIO that drives the WAL behavior at low temperatures. Further studies should help disentangle the roles of strain relaxation, oxygen vacancies, and localized moments that drive the metal-to-insulator behavior in SIO, and the possible magnetic states that may emerge in strained films. Density functional theory and dynamical mean-field theory modeling of the effects of oxygen vacancies on carrier behavior in SIO would also be worthwhile.

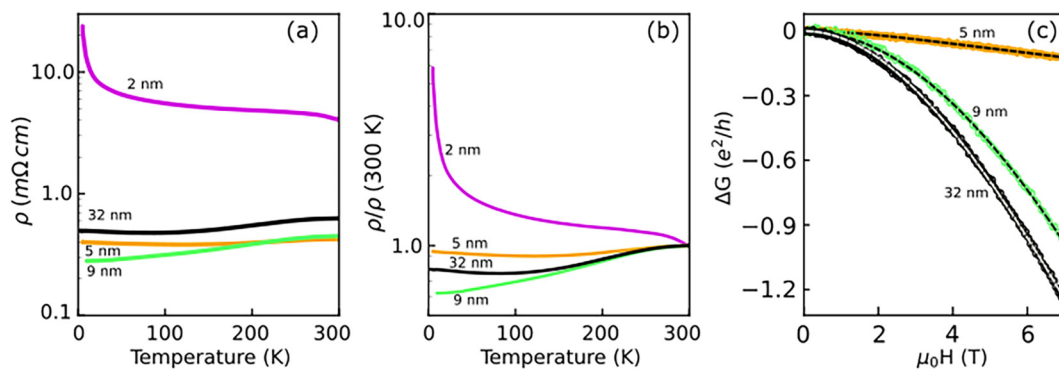


FIG. 4. (a) Resistivity vs temperature for SIO films on LSAT. (b) The same data normalized to room-temperature resistivity to emphasize temperature-dependent behavior. (c) Magnetoconductance of the same films at 5 K. The dashed lines are fits to the HLN model.

**Conclusion.** In summary, we show a systematic metal-to-insulator transition in epitaxially strained SrIrO<sub>3</sub> films. Higher compressive strain is found to show metallic behavior while lower compressive strain and even a slight tensile strain results in insulating states. The observation of Kondo behavior in resistivity shows the presence of localized magnetic states associated with strain, which likely arise due to oxygen vacancies. Our results suggest a proximity of the strained  $n = \infty$  perovskite iridate to a magnetic ground state and a quantum critical point that can be tuned via strain and oxygen vacancy concentrations. Further work could explore alternative avenues to electron-dope SrIrO<sub>3</sub> to examine how the tuning of electron concentrations can be used to control the strength of Kondo scattering and the emergence of a Kondo insulating state in the material.

**Acknowledgments.** We thank Bharat Jalan for helpful discussions. We thank Tamara Isaacs-Smith for

performing Rutherford backscattering measurements. Research at Auburn University was supported by the U.S. Department of Energy (DOE), Office of Science, Basic Energy Sciences (BES), under Award No. DE-SC0023478 (film synthesis, x-ray diffraction, and electrical transport, G.R. and R.B.C.) and by the National Science Foundation (NSF) under Award No. DMR-2045993 (x-ray photoelectron spectroscopy, T.T.). X-ray diffraction measurements were performed at Auburn on a system supported by the NSF Major Research Instrumentation (MRI) program under Award No. DMR-2018794. G.C.O. and J.H. acknowledge funding support from NSF under Award No. DMR-1847964 (electron microscopy). This research used resources from the Advanced Photon Source, an Office of Science User Facility operated for the U.S. Department of Energy (DOE) Office of Science by Argonne National Laboratory and was supported by the U.S. DOE under Contract No. DE-AC02-06CH11357.

- 
- [1] Y. Tokura, M. Kawasaki, and N. Nagaosa, Emergent functions of quantum materials, *Nat. Phys.* **13**, 1056 (2017).
- [2] W. Witczak-Krempa, G. Chen, Y. B. Kim, and L. Balents, Correlated quantum phenomena in the strong spin-orbit regime, *Annu. Rev. Condens. Matter Phys.* **5**, 57 (2014).
- [3] H. Y. Hwang, Y. Iwasa, M. Kawasaki, B. Keimer, N. Nagaosa, and Y. Tokura, Emergent phenomena at oxide interfaces, *Nat. Mater.* **11**, 103 (2012).
- [4] J. Falson and M. Kawasaki, A review of the quantum Hall effects in MgZnO/ZnO heterostructures, *Rep. Prog. Phys.* **81**, 056501 (2018).
- [5] G. Cao and P. Schlottmann, The challenge of spin-orbit-tuned ground states in iridates: A key issues review, *Rep. Prog. Phys.* **81**, 042502 (2018).
- [6] C. Lu and J. M. Liu, The  $J_{\text{eff}} = 1/2$  antiferromagnet Sr<sub>2</sub>IrO<sub>4</sub>: A golden avenue toward new physics and functions, *Adv. Mater.* **32**, 1904508 (2020).
- [7] J. G. Rau, E. K.-H. Lee, and H.-Y. Kee, Spin-orbit physics giving rise to novel phases in correlated systems: Iridates and related materials, *Annu. Rev. Condens. Matter Phys.* **7**, 195 (2016).
- [8] F. A. Wang and T. Senthil, Twisted Hubbard model for Sr<sub>2</sub>IrO<sub>4</sub>: Magnetism and possible high temperature superconductivity, *Phys. Rev. Lett.* **106**, 136402 (2011).
- [9] D. Haskel, G. Fabbris, J. H. Kim, L. S. I. Veiga, J. R. L. Mardegan, C. A. Escanhoela, S. Chikara, V. Struzhkin, T. Senthil, B. J. Kim, G. Cao, and J. W. Kim, Possible quantum paramagnetism in compressed Sr<sub>2</sub>IrO<sub>4</sub>, *Phys. Rev. Lett.* **124**, 067201 (2020).
- [10] M. A. Zeb and H.-Y. Kee, Interplay between spin-orbit coupling and Hubbard interaction in SrIrO<sub>3</sub> and related *Pbnm* perovskite oxides, *Phys. Rev. B* **86**, 085149 (2012).
- [11] G. Cao, J. E. Crow, R. P. Guertin, P. F. Henning, C. C. Homes, M. Strongin, D. N. Basov, and E. Lochner, Charge density wave formation accompanying ferromagnetic ordering in quasi-one-dimensional BaIrO<sub>3</sub>, *Solid State Commun.* **113**, 657 (2000).
- [12] D. G. Schlom, Perspective: Oxide molecular-beam epitaxy rocks!, *APL Mater.* **3**, 062403 (2015).
- [13] S. Thapa, R. Paudel, M. D. Blanchet, P. T. Gemperline, and R. B. Comes, Probing surfaces and interfaces in complex oxide films via *in situ* x-ray photoelectron spectroscopy, *J. Mater. Res.* **36**, 26 (2021).
- [14] G. Rimal and R. B. Comes, Advances in complex oxide quantum materials through new approaches to molecular beam epitaxy, *J. Phys. D: Appl. Phys.* **57**, 193001 (2024).
- [15] Y. F. Nie, P. D. C. King, C. H. Kim, M. Uchida, H. I. Wei, B. D. Faeth, J. P. Ruf, J. P. C. Ruff, L. Xie, X. Pan, C. J. Fennie, D. G. Schlom, and K. M. Shen, Interplay of spin-orbit interactions, dimensionality, and octahedral rotations in semimetallic SrIrO<sub>3</sub>, *Phys. Rev. Lett.* **114**, 016401 (2015).
- [16] R. Choudhary, S. Nair, Z. Yang, D. Lee, and B. Jalan, Semi-metallic SrIrO<sub>3</sub> films using solid-source metal-organic molecular beam epitaxy, *APL Mater.* **10**, 091118 (2022).
- [17] J. M. Longo, J. A. Kafalas, and R. J. Arnett, Structure and properties of the high and low pressure forms of SrIrO<sub>3</sub>, *J. Solid State Chem.* **3**, 174 (1971).
- [18] See Supplemental Material at <http://link.aps.org/supplemental/10.1103/PhysRevMaterials.8.L071201> for additional data, including scanning transmission electron microscopy, x-ray absorption spectroscopy, x-ray photoelectron spectroscopy, Rutherford backscattering, and transport measurements.
- [19] X. Liu, Y. Cao, B. Pal, S. Middey, M. Kareev, Y. Choi, P. Shafer, D. Haskel, E. Arenholz, and J. Chakhalian, Synthesis and electronic properties of Ruddlesden-Popper strontium iridate epitaxial thin films stabilized by control of growth kinetics, *Phys. Rev. Mater.* **1**, 075004 (2017).
- [20] R. Chaurasia, K. Asokan, K. Kumar, and A. K. Pramanik, Low-temperature ferromagnetism in perovskite SrIrO<sub>3</sub> films, *Phys. Rev. B* **103**, 064418 (2021).
- [21] G. Cao, V. Durairaj, S. Chikara, L. E. DeLong, S. Parkin, and P. Schlottmann, Non-Fermi-liquid behavior in nearly ferromagnetic SrIrO<sub>3</sub> single crystals, *Phys. Rev. B* **76**, 100402(R) (2007).
- [22] A. Biswas, K.-S. Kim, and Y. H. Jeong, Metal insulator transitions in perovskite SrIrO<sub>3</sub> thin films, *J. Appl. Phys.* **116**, 213704 (2014).
- [23] J. Liu, J.-H. Chu, C. R. Serrao, D. Yi, J. Koralek, C. Nelson, C. Frontera, D. Kriegner, L. Horak, E. Arenholz, J. Orenstein,

- A. Vishwanath, X. Marti, and R. Ramesh, Tuning the electronic properties of  $J_{\text{eff}} = 1/2$  correlated semimetal in epitaxial perovskite  $\text{SrIrO}_3$ , [arXiv:1305.1732](#).
- [24] J. Yang, L. Hao, D. Meyers, T. Dasa, L. Xu, L. Horak, P. Shafer, E. Arenholz, G. Fabbris, Y. Choi, D. Haskel, J. Karapetrova, J.-W. Kim, P. J. Ryan, H. Xu, C. D. Batista, M. P. M. Dean, and J. Liu, Strain-modulated Slater-Mott crossover of pseudospin-half square-lattice in  $(\text{SrIrO}_3)_1/(\text{SrTiO}_3)_1$  superlattices, *Phys. Rev. Lett.* **124**, 177601 (2020).
- [25] K.-H. Kim, H.-S. Kim, and M. J. Han, Electronic structure and magnetic properties of iridate superlattice  $\text{SrIrO}_3/\text{SrTiO}_3$ , *J. Phys.: Condens. Matter* **26**, 185501 (2014).
- [26] D. J. Groenendijk, C. Autieri, J. Girovsky, M. C. Martinez-Velarte, N. Manca, G. Mattoni, A. M. R. V. L. Monteiro, N. Gauquelin, J. Verbeeck, A. F. Otte, M. Gabay, S. Picozzi, and A. D. Caviglia, Spin-orbit semimetal  $\text{SrIrO}_3$  in the two-dimensional limit, *Phys. Rev. Lett.* **119**, 256403 (2017).
- [27] M. Lee, J. R. Williams, S. Zhang, C. D. Frisbie, and D. Goldhaber-Gordon, Electrolyte gate-controlled Kondo effect in  $\text{SrTiO}_3$ , *Phys. Rev. Lett.* **107**, 256601 (2011).
- [28] X. Cai, J. Yue, P. Xu, B. Jalan, and V. S. Pribiag, From weak antilocalization to Kondo scattering in a magnetic complex oxide interface, *Phys. Rev. B* **103**, 115434 (2021).
- [29] T. A. Costi, A. C. Hewson, and V. Zlatic, Transport coefficients of the Anderson model via the numerical renormalization group, *J. Phys.: Condens. Matter* **6**, 2519 (1994).
- [30] J. Kondo, Resistance minimum in dilute magnetic alloys, *Prog. Theor. Phys.* **32**, 37 (1964).
- [31] J.-G. Cheng, J.-S. Zhou, Y.-F. Yang, H. D. Zhou, K. Matsubayashi, Y. Uwatoko, A. MacDonald, and J. B. Goodenough, Possible Kondo physics near a metal-insulator crossover in the A-site ordered perovskite  $\text{CaCu}_3\text{Ir}_4\text{O}_{12}$ , *Phys. Rev. Lett.* **111**, 176403 (2013).
- [32] C. Lin and A. A. Demkov, Consequences of oxygen-vacancy correlations at the  $\text{SrTiO}_3$  interface, *Phys. Rev. Lett.* **113**, 157602 (2014).
- [33] H. Zheng, J. Terzic, F. Ye, X. G. Wan, D. Wang, J. Wang, X. Wang, P. Schlottmann, S. J. Yuan, and G. Cao, Simultaneous metal-insulator and antiferromagnetic transitions in orthorhombic perovskite iridate  $\text{Sr}_{0.94}\text{Ir}_{0.78}\text{O}_{2.68}$  single crystals, *Phys. Rev. B* **93**, 235157 (2016).
- [34] Q. Cui, J.-G. Cheng, W. Fan, A. E. Taylor, S. Calder, M. A. McGuire, J.-Q. Yan, D. Meyers, X. Li, Y. Q. Cai, Y. Y. Jiao, Y. Choi, D. Haskel, H. Gotou, Y. Uwatoko, J. Chakhalian, A. D. Christianson, S. Yunoki, J. B. Goodenough, and J.-S. Zhou, Slater insulator in iridate perovskites with strong spin-orbit coupling, *Phys. Rev. Lett.* **117**, 176603 (2016).
- [35] U. Aschauer, R. Pfenninger, S. M. Selbach, T. Grande, and N. A. Spaldin, Strain-controlled oxygen vacancy formation and ordering in  $\text{CaMnO}_3$ , *Phys. Rev. B* **88**, 054111 (2013).
- [36] B. Kim, P. Liu, and C. Franchini, Magnetic properties of bilayer  $\text{Sr}_3\text{Ir}_2\text{O}_7$ : Role of epitaxial strain and oxygen vacancies, *Phys. Rev. B* **95**, 024406 (2017).
- [37] M. E. Sweers, Q. Ma, P. M. Donahue, D. Nordlund, S. M. Haile, and L. C. Seitz, Epitaxial strain-tuned oxygen vacancy formation, reduction behavior, and electronic structure of perovskite  $\text{SrIrO}_3$ , *Phys. Rev. Mater.* **8**, 055801 (2024).
- [38] L. Hao, D. Meyers, C. Frederick, G. Fabbris, J. Yang, N. Traynor, L. Horak, D. Kriegner, Y. Choi, J.-W. Kim, D. Haskel, P. J. Ryan, M. P. M. Dean, and J. Liu, Two-dimensional  $J_{\text{eff}} = 1/2$  antiferromagnetic insulator unraveled from interlayer exchange coupling in artificial perovskite iridate superlattices, *Phys. Rev. Lett.* **119**, 027204 (2017).
- [39] D. Gong, J. Yang, L. Hao, L. Horak, Y. Xin, E. Karapetrova, J. Stremper, Y. Choi, J.-W. Kim, P. J. Ryan, and J. Liu, Reconciling monolayer and bilayer  $J_{\text{eff}} = 1/2$  square lattices in hybrid oxide superlattice, *Phys. Rev. Lett.* **129**, 187201 (2022).
- [40] N. Bagués, J. Santiso, B. D. Esser, R. E. Williams, D. W. McComb, Z. Konstantinovic, L. Balcells, and F. Sandiumenge, The misfit dislocation core phase in complex oxide heteroepitaxy, *Adv. Funct. Mater.* **28**, 1704437 (2018).
- [41] S. Hikami, A. I. Larkin, and Y. Nagaoka, Spin-orbit interaction and magnetoresistance in the two dimensional random system, *Prog. Theor. Phys.* **63**, 707 (1980).